Research, Society and Development, v. 13, n. 1, e3213144702, 2024
(CC BY 4.0) | ISSN 2525-3409 | DOI: http://dx.doi.org/10.33448/rsd-v13i1.44702

Discrete pore and particle size distributions during pore blocking and cake filtration

Distribuição discreta de poros e das partículas durante o bloqueio de poros e a filtração do reboco

Distribución discreta de los poros y de las partículas durante el bloqueo de poros y la filtración del revoque

Received: 12/20/2023 | Revised: 12/31/2023 | Accepted: 01/03/2024 | Published: 01/06/2024

Jhon Moron Tarifa
ORCID: https://orcid.org/0000-0002-5366-1289
Federal University of Rio Grande do Norte, Brazil
E-mail: jhon.tarifa.704@ufrn.edu.br
Adriano dos Santos
ORCID: https://orcid.org/0000-0003-1745-9152
Federal University of Rio Grande do Norte, Brazil
E-mail: adriano.santos@ufrn.br

Abstract
Modeling membrane filtration is important for plenty industrial applications. The understanding of the phenomena and related mechanisms aims at the improvement of techniques in different areas. Therefore, different authors have proposed models to describe the mechanisms related to the filtration process involving either cake build-up or blocking processes, a few of them however have proposed both concepts simultaneously, although none considered pore and particle size distribution during the process, which is the proposal brought up in this paper. Transient solutions for filtrate volume and filter cake thickness as a function of initial pore and particle size distributions are obtained. Good matching between the studied experimental data and the proposed model was observed. In general, the results showed that permeability reduction and filtrate volume are strongly influenced by the initial pore and particle size distributions. In addition, the cake build-up rate depends on both the particle size distribution and the residual flow through blocked pores. It was observed that, after all the largest particles have blocked the smaller pores, effective permeability and flow rate vary only due to cake build-up. Finally, because the proposed empirical parameters do not depend on the pore size distribution, this model can be applied for predicting permeability decline for any feed concentration.
Keywords: Microfiltration; Straining; Pore blocking; Cake build-up; Pore and particle size distributions.

Resumo
A modelagem da filtração através de membranas é importante para muitas aplicações na indústria, o entendimento dos fenômenos e mecanismos relacionados visam o aprimoramento das técnicas em diferentes áreas. Por conseguinte, vários autores propuseram modelos para descrever os mecanismos relacionados ao processo de filtração envolvendo tanto o crescimento do reboco quanto os processos de bloqueio, não entanto, poucos deles propuseram ambos os conceitos simultaneamente, embora nenhum considere a distribuição do tamanho de poros e das partículas durante o processo, o que é a proposta apresentada neste artigo. Soluções transientes para o volume filtrado e a espessura do reboco foram encontradas em função da distribuição inicial do tamanho dos poros e das partículas. Um bom ajuste entre os dados experimentais estudados e o modelo proposto foi observado. Em geral, os resultados mostraram que a redução da permeabilidade e do volume filtrado são fortemente influenciados pela distribuição inicial do tamanho dos poros e das partículas. Adicionalmente, a taxa de crescimento do reboco depende da distribuição do tamanho das partículas e do fluxo residual dos poros bloqueados. Foi observado que, depois que todos os poros menores que as maiores partículas são bloqueados, a permeabilidade efetiva e a taxa de fluxo variam dependendo do crescimento do reboco. Finalmente, como os parâmetros empíricos propostos não dependem da distribuição do tamanho dos poros, o modelo proposto pode ser usado para predizer o declínio da permeabilidade para qualquer concentração.
Palavras-chave: Microfiltração; Straining; Bloqueio de poros; Crescimento do reboco; Distribuição do tamanho dos poros e das partículas.

Resumen
El modelaje de la filtración a través de las membranas es importante para muchas aplicaciones en la industria y el entendimiento de los fenómenos y mecanismos relacionados tienen como objetivo el perfeccionamiento de las técnicas en diferentes áreas. Consecuentemente, varios autores propusieron modelos para describir los mecanismos relacionados al proceso de filtración envolviendo tanto el crecimiento del revoque cuanto los procesos de bloqueo, sin embargo, pocos de ellos propusieron ambos procesos simultáneamente, aunque ninguno lleve en consideración la

distribución del tamaño de los poros y de las partículas durante el proceso, la cual es la propuesta de este artículo. Soluciones transientes para el volumen filtrado y para la espesura del revoque fueron encontradas en función de la distribución inicial del tamaño de los poros y de las partículas. Un buen ajuste entre los datos experimentales estudiados y el modelo propuesto fue observado. En general, los resultados mostraron que la reducción de la permeabilidad y del volumen filtrado son fuertemente influenciados por la distribución inicial del tamaño de los poros y de las partículas. Adicionalmente, la tasa de crecimiento del revoque depende de la distribución del tamaño de las partículas y del flujo residual de los poros bloqueados. Fue observado que después que todos los poros más pequeños que las mayores partículas son bloqueados, la permeabilidad efectiva y la tasa de flujo varían dependiendo del crecimiento del revoque. Finalmente, como los parámetros empíricos propuestos no dependen de la distribución del tamaño de los poros, el modelo propuesto puede ser usado para predecir el declínio de la permeabilidad para cualquier concentración.
Palabras clave: Microfiltración; Straining; Bloqueo de poros; Crecimiento del revoque; Distribución del tamaño de los poros y de las partículas.

1. Introduction

Understanding transport of particulate suspensions in porous media is important for a variety of environmental, industrial, chemical and petroleum technologies. It takes place in industrial filtering, size exclusion chromatography, industrial waste disposal, wastewater treatment, water filtration, waterflooding in petroleum reservoirs, etc.

During membrane microfiltration, particles are retained due to different mechanisms such as straining, electric forces, diffusion and bridging. The effectiveness of each particle retention mechanism depends on the interaction forces between the porous media, the injected fluid and the suspended particles. Therefore, parameters such as flow rate, particle concentration, particle and pore size distributions, the interaction energies (particles-particles and particles-pores) and the fluid composition can determine the most effective particle retention mechanisms (Herzig et al., 1970; Santos & Bedrikovetsky, 2004; Sharma & Yortsos, 1987).

If the solid matrix of a porous medium is deformable, its porous structure may change during flow or some other transport phenomenon. If the fluid is reactive or carries solid particles of various shapes, sizes, and electrical charges, the pore structure of the medium may change due to the reaction of the fluid with the pore surface, or the physicochemical interaction between the particles and the pore surface.

Straining mechanism occurs when a particle encounters a pore smaller than itself. In this case, pores are completely or partially blocked resulting in permeability reduction (Kosvintsev et al., 2004; Kosvintsev et al., 2002; Filippov et al., 1994; Santos & Bedrikovetsky, 2004; Shapiro et al., 2007).

In order to model membrane resistance during microfiltration, the following mechanisms (Gonsalves, 1950; Grace, 1956; Hermans et al., 1935) were suggested: (a) standard model (internal pore constriction due to particle retention); (b) intermediate pore blocking (partial pore blocking); (c) complete pore blocking (particle completely blocks a pore); (d) cake filtration (particles accumulate on the membrane surface). Several authors (Gonsalves, 1950; Hlavacek & Bouchet, 1993) have proposed empirical laws for membrane microfiltration considering the afore mentioned fouling mechanisms. Hlavacek and Bouchet, 1993; and Tracey and Davis, 1994; observed that pore blocking models showed good agreement with experimental data for BSA (Bovine serum albumin) injection during membrane (cellullose, track-etched polycarbonate e PVDF) microfiltration. In addition, the afore mentioned authors suggested that, after the initial pore blocking stage, cake filtration is the dominant fouling mechanism. On the other hand, Bowen et al., 1995; observed that single blocking models are not able to fit experimental data and suggested that multiple pore-blocking mechanisms are operative during membrane microfiltration. Combining the equations for the afore mentioned mechanisms, Bolton et al. 2006; observed a good fitting with experimental data.

Ho e Zydney, 1995; proposed a model for simultaneous pore blocking and cake build-up. The model, which assumes flow through partially blocked pores, presented a good agreement with the studied experimental data. However, it is important

to highlight that the afore mentioned models do not take particle and pore size distributions into account. Therefore, they are not predictive because the relationships between empirical constants and the particle and pore size distributions are unknown. In other words, each combination of particle and pore size distribution will result in different model coefficients (which should be experimentally determined). Alternatively, models for membrane pore blocking taking particle and pore size distributions into account have been proposed in the literature (Santos & Bedrikovetsky, 2006; Santos et al., 2008), but even those models don't seem to respond adequately when the cake is formed.

Models that take pore and particle size distribution into account could be divided into two groups: the continuum models and the discrete or network models (models for flow, dispersion, and displacement processes in porous media). A comparison between them is out of the scopus of this article, nevertheless, the continuum models have some limitations, concerning scales and averaging. Also, phenomena in which the connectivity of the pore space, or where fluid phase plays a major role are not well adapted. Continuum models also fail if there are correlations in the system with an extent that is comparable with the linear size of the porous medium (Santos & Bedrikovetsky, 2006; Santos et al., 2008).

Discrete models describe phenomena at the microscopic level and have been extended to describe various phenomena at the macroscopic and even larger scales. From a practical point of view, the large computational effort required for a realistic discrete treatment of the pore space is the main deficiency. They are particularly useful when the effect of the pore space connectivity is strong (Santos & Bedrikovetsky, 2006; Santos et al., 2008).

A model proposed by Santos et al. (Santos & Bedrikovetsky, 2006; Santos et al., 2008), which incorporates both discrete pore and particle size distributions (laboratory data is better presented as discrete, i.e. pore and particle radius can be measured), is studied and used as our base to propose analytical solutions.

Flow phenomena only in a static medium was studied, that is, during a given process no change in the morphology occurred. Therefore, deformable media as well as those physicochemical interactions between the particle and pore surface and a fluid, or those expected to undergo morphological changes due to a chemical reaction, are not studied here.

In this article, a predictive model for simultaneous pore blocking and cake build-up is proposed. The obtained solutions, which are strongly dependent on the particle and pore size distributions, showed good agreement with the studied experimental data.

2. Methodology

2.1 Modeling Simultaneous Pore Blocking and Cake Filtration

In this section, the governing equations for a predictive model considering simultaneous pore blocking and cake build-up are presented.

Various authors (Filippov et al., 1994; Santos & Bedrikovetsky, 2004; Shapiro et al., 2007; Sharma & Yortsos, 1987) have proposed pore blocking kinetics taking pore and particle size distributions into account. Following Sharma and Yortsos, 1987; and Santos et al. (Santos et al., 2004; Santos et al., 2006), the following pore blocking kinetics during straining of polydisperse particulate suspensions was considered:

$$\frac{\partial H}{\partial t} = -\lambda \frac{U\ r_p^4 H}{\int_0^\infty r_p^4 H dr_p} \int_{r_p}^\infty C dr_s \tag{1}$$

where:

$$\Lambda = \frac{\pi}{8\mu} \frac{\Delta P}{L_m} \tag{2}$$

The above equation was derived considering Poiseuille flow through a bundle of parallel tubes distributed over radii.

In addition, μ is the fluid viscosity; ΔP is the pressure drop across the membrane; L_m is the membrane thickness. Moreover, H and C represent open-pore and suspended-particle size distributions, respectively; r_p and r_s are pore and particle sizes, respectively; the term $\int_{r_p}^{\infty} C dr_s$ represents the amount of particles larger than r_p and Q represents flow rate, defined as:

$$Q = \frac{dV}{dt} \tag{3}$$

Where V is the filtrate volume.

In order to discretize equation (1), Santos et al., 2008; proposed to represent pore and particle size distributions by using the Dirac delta functions (δ), as follows:

$$H(r_p, x, t) = \sum_{i=1}^{N} h_i \delta(r_p - r_{p,i}) \tag{4}$$

$$C(r_s, x, t) = \sum_{i=1}^{n} c_i \delta(r_s - r_{s,i}) \tag{5}$$

Where h_i is the open-pore concentration with radius $r_{p,i}$ (*number of open-pores with radius* $r_{p,i}$ *per unit of membrane area*) and c_i is the particle concentration with radius $r_{s,i}$ (*number of particles with radius* $r_{s,i}$ *per unit of fluid volume*). In addition, $r_{s,n}$ represents the radius of the largest particle in suspension and $r_{p,N}$ represents the largest pore radius. Figure 1 shows a sketch of pore and particle size distributions. Notice that particle and pore size distributions are non-zero only for radii equals $r_{s,i}$ and $r_{p,j}$ (with $1 \leq i \leq n$ and $1 \leq j \leq N$), respectively. In addition, it is worth mentioning that pores with radius $r_{p,i}$ can be blocked by particles with radii $r_{s,i}, r_{s,i+1}, \cdots, r_{s,n}$.

Figure 1 - Initial distribution of pore and particle.

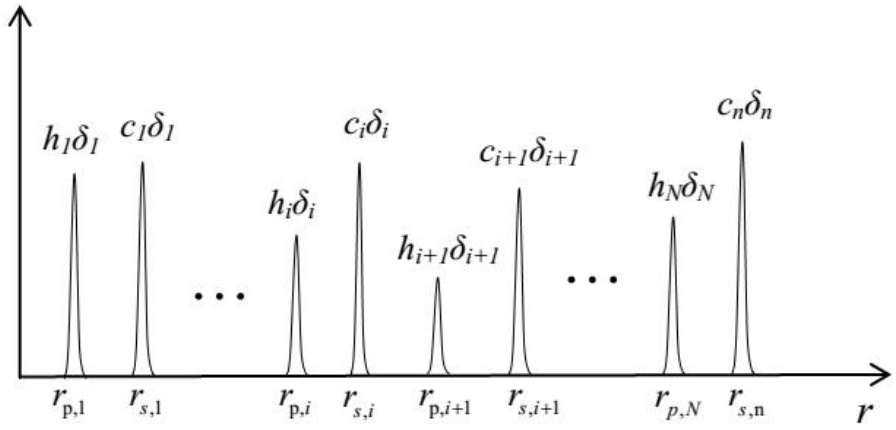

Source: Authors.

Substituting pore and particle distributions defined by Eqs. (4) and (5) into eq.(1) and integrating the resulting equation from $r_{s,i-1}$ to $r_{s,i}$ (with $r_{s,0} = 0$), it follows that:

$$\frac{\partial \tilde{h}_i}{\partial t} = -\lambda U \frac{c_0}{h_0} \frac{r_{p,i}^4 \tilde{h}_i}{\sum_{i=1}^{N} r_{p,i}^4 \tilde{h}_i} \sum_{j=i}^{n} \tilde{c}_j \tag{6}$$

Where $\tilde{h}_i$ is the fraction of pores with size $r_{p,i}$ and $\tilde{c}_j$ is the fraction of particles with size $r_{s,j}$ and c_0 is the number of injected particles per unit of fluid volume.

Defining $\tilde{h}_{i,0} (\tilde{h}_i = \frac{h_i}{h_0})$ as the initial concentration of pores with radius $r_{p,i}$, the following initial condition is stated:

$$t = 0 \quad ; \quad \tilde{h}_i = \tilde{h}_{i,0} \tag{7}$$

Integrating Eq. (6), considering constant pressure drop and initial conditions (7), results in:

$$\tilde{h}_i(t) = \begin{cases} \tilde{h}_{i,0} exp\left[-\lambda c_0 \Lambda t r_{p,i}^4 \sum_{j=i}^{n} \tilde{c}_j\right] & ; \ i \leq n \\ \tilde{h}_{i,0} & ; \ i > n \end{cases} \quad (8)$$

As expected, the equation (8) shows that, if there exists pores larger than the largest particle $(r_{p,i} > r_{s,n})$, they are never blocked by straining. On the other hand, smaller pores are blocked, and their concentrations decrease exponentially.

Considering flow rate through open pores (Q_{OP}) and "residual flow" through partially blocked pores (Q_{BP}), total flow rate is given by:

$$\frac{dV}{dt} = Q_{OP} + Q_{BP} \quad (9)$$

Assuming Poiseuille flow in each pore, flow through open pores is given by:

$$Q_{OP}(t) = \Lambda A \sum_{i=1}^{N} r_{p,i}^4 \tilde{h}_i(t) \quad (10)$$

In addition, due to pore blocking and cake build-up, resistance increases resulting in the following flow rate (Q_{BP}) through blocked area fraction (α_{BP}):

$$Q_{BP}(t) = A\alpha_{BP}(t) \frac{\Delta P}{\mu} \left[\frac{8\alpha_{BP}(t) L_m}{\pi \varepsilon^4 \sum_{i=1}^{N} r_{p,i}^4 [\tilde{h}_{i,0} - \tilde{h}_i(t)]} + \frac{L_c(t)}{k_c}\right]^{-1} \quad (11)$$

Substituting (11) and (10) into (9) results in:

$$\frac{dV}{dt} = K(t) \frac{A}{\mu} \frac{\Delta P}{L_m} \quad (12)$$

where $K(t)$ represents the effective permeability, given by:

$$K(t) = \frac{\pi}{8} \sum_{i=1}^{N} r_{p,i}^4 \tilde{h}_i(t) + \left[\frac{8}{\pi \varepsilon^4 \sum_{i=1}^{N} r_{p,i}^4 [\tilde{h}_{i,0} - \tilde{h}_i(t)]} + \frac{L_c(t)}{k_c \alpha_{BP}(t) L_m}\right]^{-1} \quad (13)$$

Assuming that spatial distribution of pores is uniform, it follows that:

$$\alpha_{BP}(t) = \frac{\sum_{i=1}^{N} [\tilde{h}_{i,0} - \tilde{h}_i(t)]}{\sum_{i=1}^{N} \tilde{h}_{i,0}} \quad (14)$$

In addition, "$\tilde{h}_{i,0} - \tilde{h}_i(t)$" represents the concentration (number per unit of membrane area) of pores of size $r_{p,i}$ which were blocked and acquired a hydraulic radius $\tilde{r}_{p,i}$ and $\varepsilon = \frac{\tilde{r}_{p,i}}{r_{p,i}}$ is the blocked-to-unblocked pore size ratio; which can be obtained empirically or derived by assuming a given particle and pore geometry. Furthermore, constant cake permeability (k_c) and porosity (ϕ_c) were assumed. Considering mass balance during cake accumulation, it follows that cake thickness (L_c) is given by:

$$L_c(t) = \frac{\frac{4}{3}\pi \sum_{i=1}^{n} r_{s,j}^3 f_{s,j} \int_0^t Q_{BP}\, dt}{\alpha_{BP}(t) A (1 - \phi_c)} \quad (15)$$

Membrane surface during pore blocking and cake build-up is presented in Figures 2a and 2b and a sketch of the afore mentioned process is shown in Figures 2c and 2d. It is important to notice that cake growth can only be explained if residual flow is considered. Otherwise, flow through blocked pores would tend to zero and external cake build-up could not occur.

Figure 2 - Scanning electron microscope showing the membrane surface (a) and the particles accumulated on the cake (b); sketch of pore blocking (c) and external cake build-up (d).

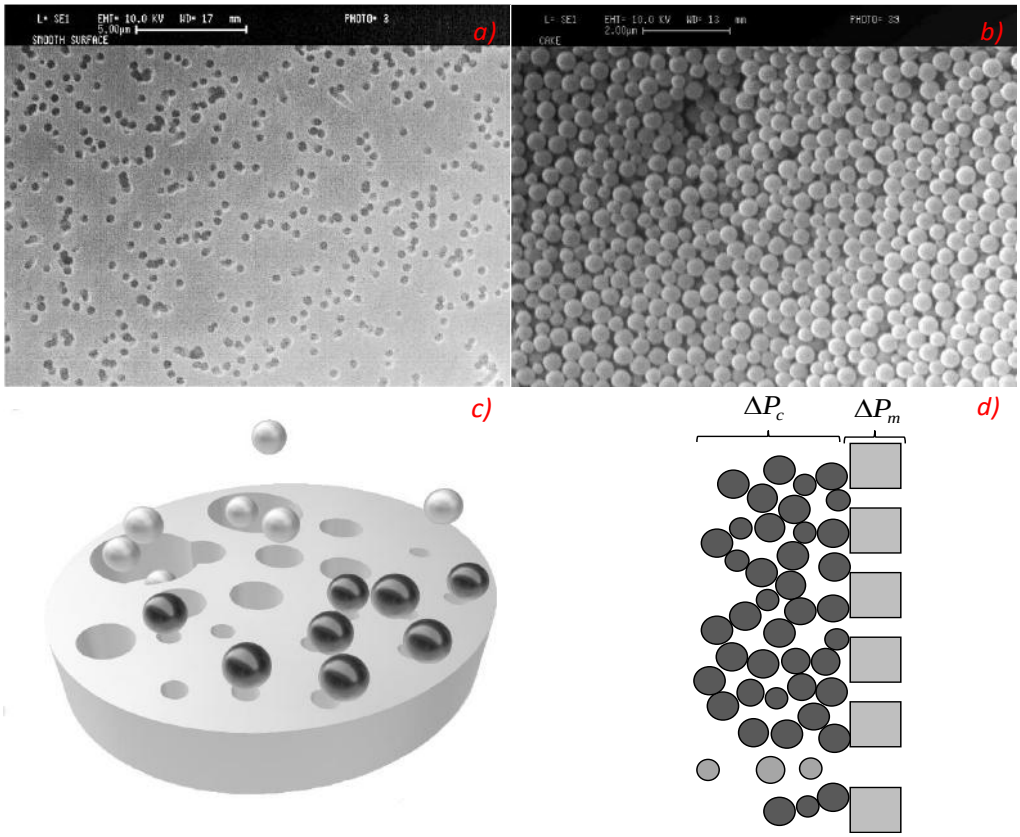

Source: Adapted from Kosvintsev et al. (2002) and Kosvintsev et al. (2004).

Finally, in order to calculate $V(t)$, equation (12) is solved by using the third order Runge-Kutta method.

It is well known that cake resistance dominates after the initial pore blocking period (Ho & Zydney, 2000; Kosvintsev et al., 2002). In the limiting case, after all pores smaller than the largest particle are blocked, from (8) and (12), it follows that:

$$K(t) = \frac{\pi}{8}\sum_{i=n+1}^{N} r_{p,i}^4 \tilde{n}_{i,0} + \left[\frac{8}{\pi\varepsilon^4 \sum_{i=1}^{n} r_{p,i}^4 \tilde{n}_{i,0}} + \frac{L_c(t)}{\alpha_{BP}^* L_m k_c}\right]^{-1} \quad (16)$$

where: $\alpha_{BP}^* = \frac{\sum_{i=1}^{n} \tilde{n}_{i,0}}{\sum_{i=1}^{N} \tilde{n}_{i,0}}$

In other words, after all pores smaller than the largest particle are blocked, effective permeability and flow rate (see equations (16) and (12)) vary only due to cake growth, alternately, when small particle concentrations are considered, cake formation is not taken into account, allowing simplification in equation (9), so discrete (proposed model) and continuous model (Filippov et al., 1994) could be compared. Finally, because the Kozeny-Carman relationship between porosity and permeability is considered, the model (12)-(15) contains two fitting parameters (ϕ_c, ε). The cake porosity (ϕ_c) is a function of both particle sizes and packing. Additionally, the blocked-to-unblocked pore size ratio (ε) depends on the particle and pore geometries.

2.2 Material and Methods

The experiments conducted by Kosvintsev et al. (Kosvintsev et al. 2002; Kosvintsev et al. 2004) are briefly described as they were used to validate the model; the coefficients were obtained by fitting these studied experimental data.

In the afore mentioned experiments, track-etched membrane with a nominal pore size of 0.4 μm, thickness 10μm and

filtering diameter and 0.04 m supplied by Millipore were used. The injected particle size distributions and initial pore size distributions are presented in Figure 3.

Figure 3 - Particle and pore size distributions.

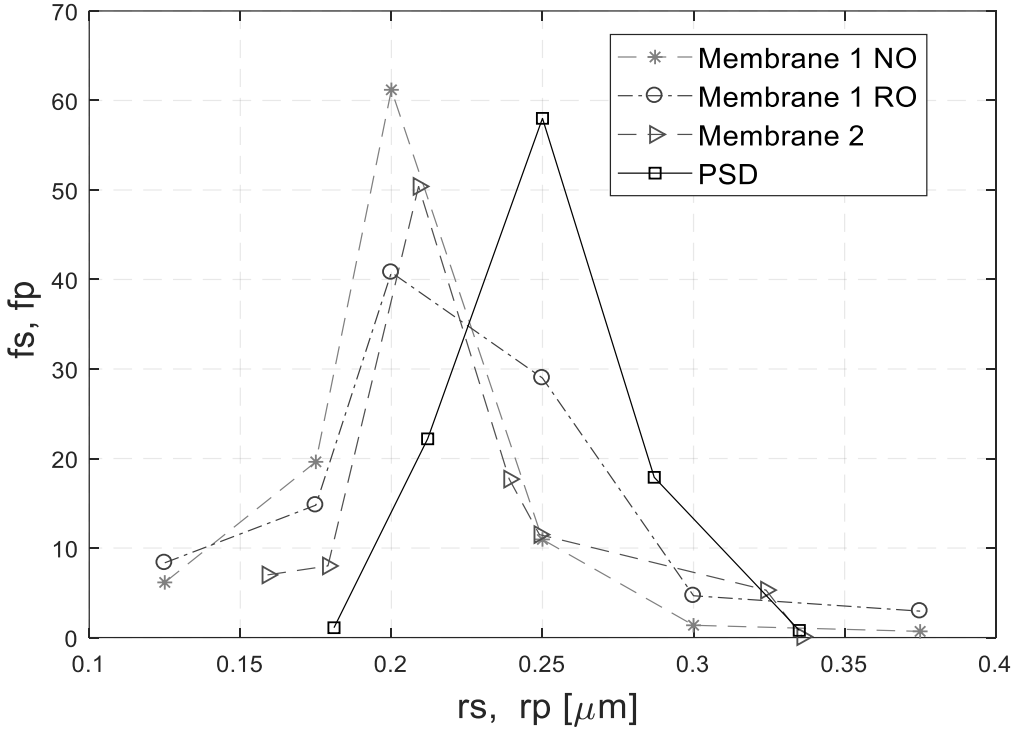

Source: Authors.

The size distribution of the suspended latex polysterene particles were measured by a Malvern Mastersizer. The mean particle diameter was 0.46 µm and 80% of particles presented diameter between 0.4 and 0.51 µm. In addition, water obtained from a MilliQ purification system was used to prepare different feed suspension concentrations (see Table 1). Finally, additional suspension and membrane characteristics like suspension, viscosity (µ), particle density ($\rho_{particle}$), filtration area (A), membrane porosity (Ø), thickness (*Lm*) and pore concentration (*h*) are presented in Table 1.

Table 1 - Additional membrane and feed suspension characteristics.

Membrane 1 (Normal orientation)		**Membrane 1 (Reverse orientation)**	**Membrane 2 (Normal orientation)**
A (m^2)	0.0138	0.0138	0.01257
Ø	0.15	0.15	0.18
µ (Pa s)	1×10^{-3}	1×10^{-3}	1×10^{-3}
$\rho_{particle}$ (kg/m^3)	1100	1100	1100
ΔP (Pa)	3290	3290	4900
$h_{0\ total}$ (pores/m^2)	1.179×10^{12}	9.873×10^{11}	1.165×10^{12}

Source: Authors.

3. Results and Discussion

In this section, the proposed model is verified by fitting the experimental data described in the previous section. Figures 4-6 present the proposed model fitting (least squares method) for experimental data considering different injected

concentrations on membranes 1 and 2. Using the dimensionless variables criteria of Kosvintsev et al., 2002; in equation (12), makes all operating data for microfiltration to be reduced to a single plot of dimensionless volume and time, resulting in a nondependent expression of the suspension concentration and operating pressure. Notice that equations (12)-(15) show that $\hat{V}$ is highly sensitive to variations on the pore and particle size distributions. However, only one measurement of particle size distribution (named fs) in the feed suspensions was presented in (Kosvintsev et al. 2002; Kosvintsev et al. 2004). In addition, only one pore size distribution measurement for each membrane type was presented in (Kosvintsev et al. 2002; Kosvintsev et al. 2004) (see Figure 3). In Table 2 and Figures 4-6, fpN and fpR represent the measured pore size distribution for membrane 1 (Normal and Reverse orientation, respectively) and fp2 represents the measured pore size distribution for membrane 2. In addition, the expected variations on the feed particle size distribution and on the commercial track etched membranes pore size distribution (represented by using subscripts A and B) are presented in Table 2 and Figures 4-6.

Table 2 - Particle and pore size distributions.

Co (w/w)	Membrane 1				Co (w/w)	Membrane 2	
	Normal	Reverse	Normal	Reverse			
	Particle SD	Particle SD	Pore SD	Pore SD		Particle SD	Pore SD
13×10^{-8}	fs	---	fpN	--	13×10^{-8}	fs	fp2
25×10^{-8}	fsNA	fsRA	fpNA	fpRA	100×10^{-7}	fs2A	fp2A
50×10^{-8}	fsNB	fsRB	fpNB	fpRB	500×10^{-7}	fs2B	fp2B
100×10^{-8}	fsNA	fs	fpNA	fpR			

Source: Authors.

Table 2 shows all the different scenarios *(with small variation on pore and particle size distributions*) plotted against the experimental data.

Notice that, because $\hat{V}$ is highly sensitive to variations on the pore and particle size distributions (which were not measured for each individual membrane and suspension), deviations from the fitting obtained by using the global fitting parameters were observed (see Table 3 and continuous lines in Figures 4-6).

Table 1 - Global fitting coefficients.

	Orientation			
	Normal		Reverse	
	ε	$\emptyset_c$	ε	$\emptyset_c$
Membrane 1	0.13	0.32	0.15	0.34
Membrane 2	0.26	0.35	--	--

Source: Authors.

Table 3 shows the global fitting parameters for the measured pore and particle size distribution, presenting a good fitting mainly at the earlier stage of the injection volume.

In Figures 4 and 5, the vertical dashed-dotted lines represent the times T_{50} and T_{90}, in which the blocked area fraction (α_{BP}, see equation (14)) equals 50% and 90%, respectively. Because T_{50} and T_{90} are smaller than 0,9 for membrane 2 (see Figure 7), they were omitted in Figure 6 and presented in Figure 7. The increasing deviation on the effective permeability (see equation (12)) when the blocked area fraction increases (see Figures 4-6) also suggests that small variations on the feed particle size distribution and/or membrane pore size distribution occurred when different concentrations were injected. Notice that, due to pore blocking, large variation on the effective membrane permeability is observed initially ($T \leq T_{90\%}$). On the other hand,

for larger times, external cake builds-up and its permeability dominates the effective membrane permeability (see equation (16)).

Figure 4 - Filtrate volume and sensitivity analysis of the proposed model considering small variations on the: (a) Membrane 1 (normal orientation) pore size distribution, (b) feed particle size distribution.

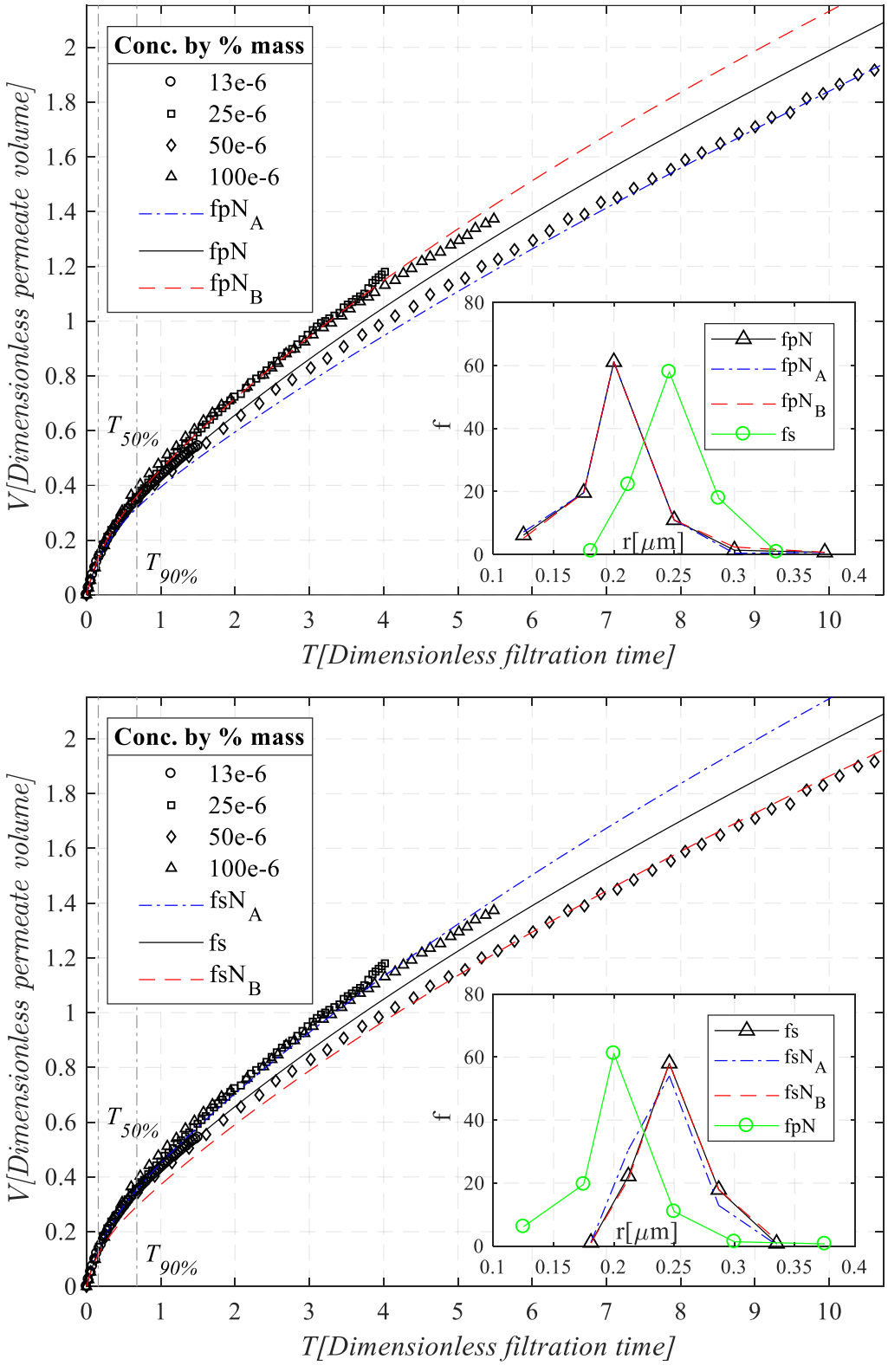

Source: Authors.

Figure 5 - Proposed model fitting and sensitivity analysis considering small variations on the: (a) Membrane 1 (reverse orientation) pore size distribution, (b) feed particle size distribution.

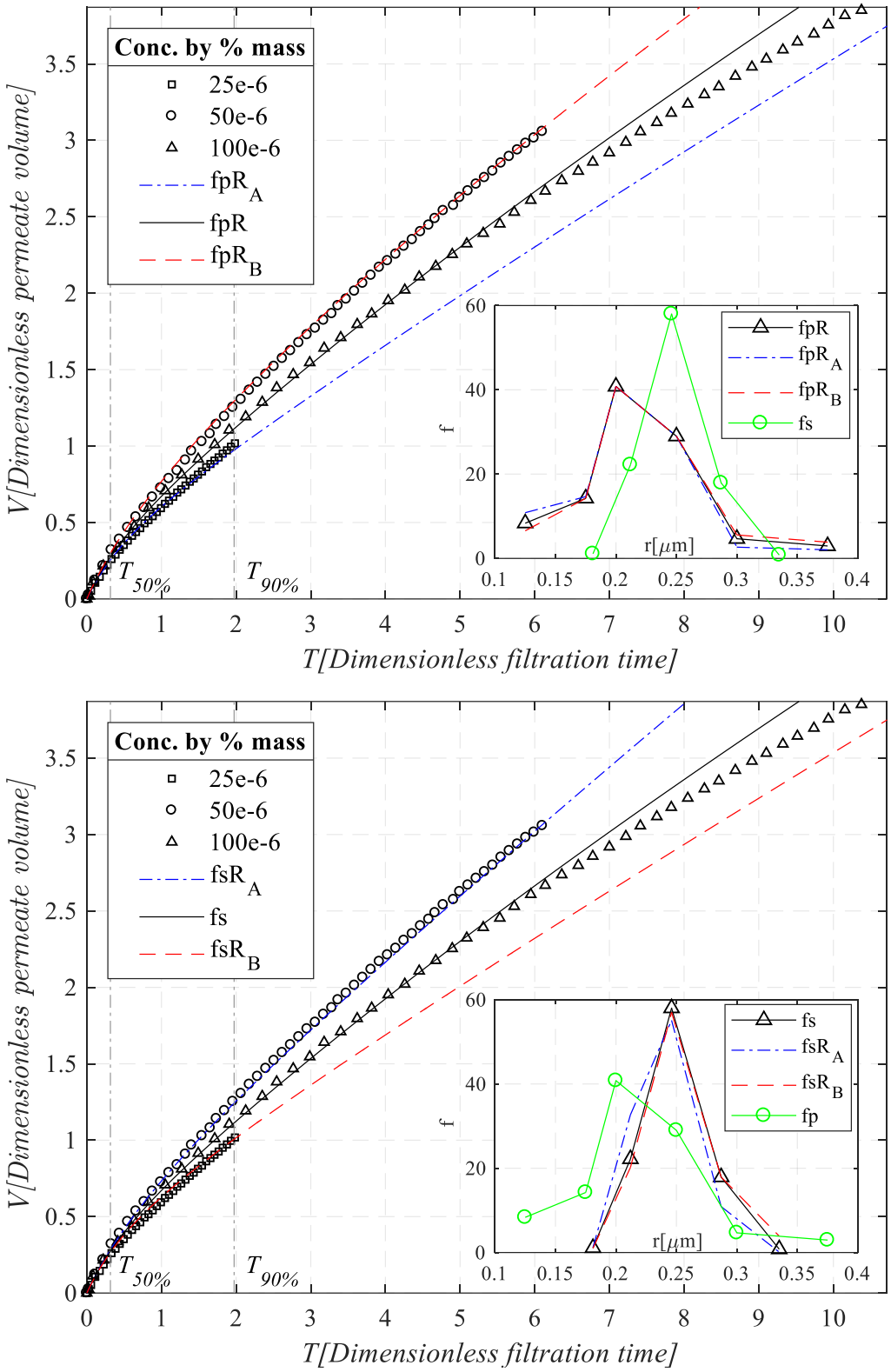

Source: Authors.

Figure 6 - Filtrate volume and sensitivity analysis considering small variations on the: (a) Membrane 2 pore size distribution, (b) feed particle size distribution.

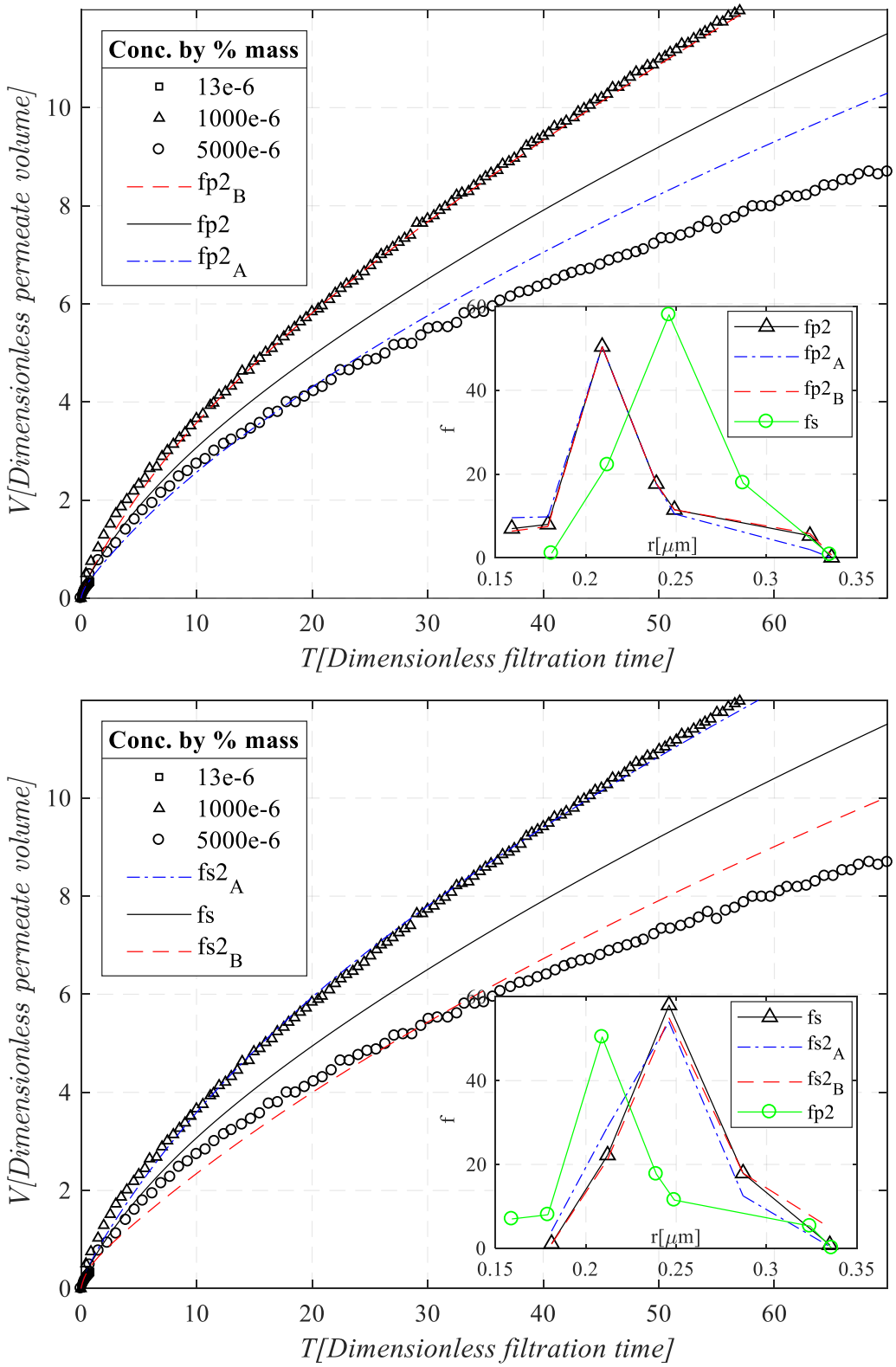

Source: Authors.

Figure 4-6 shows $\hat{V}$ (*dimensionless permeate volume*) for the proposed model (*with the global fitting parameters for the measured pore and particle size distribution*) in black continuous line. Scenarios with a small variation in the pore and

particle size distribution were considered and represented with different colors in dotted line. It can be observed that a small variation on both pore and particle size distribution presents a high influence on $\hat{V}$.

Figure 7 presents the blocked area fraction, that is highly influenced at earlier stages of the filtration process.

Figure 7 - Blocked area fraction (α_{BP}) for membrane 2.

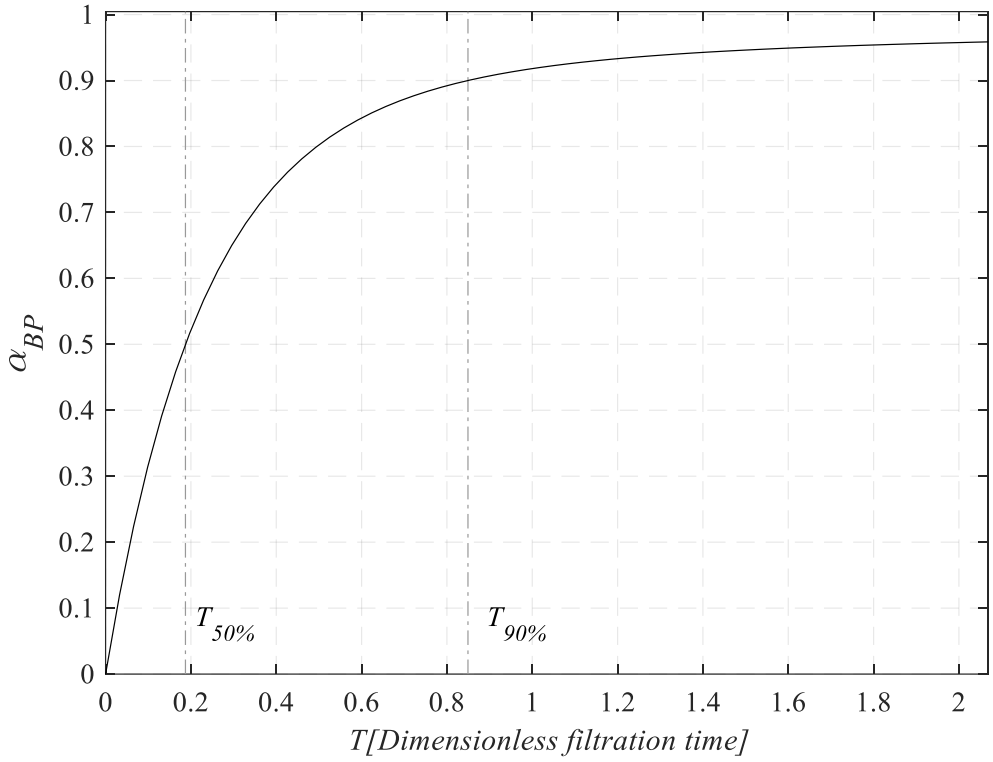

Source: Authors.

Figure 7 shows that around 90% of the pores are blocked when T=0.85. Because flow is mostly diverted to the remaining opened pores, cake build up is negligible until T=0.85 (see Figure 9) and permeability is mainly reduced due to pore blocking. However, for T=1, more than 90% of the pores are blocked and cake effect on the effective permeability becomes significant (see Figure 7 and Figure 9). Therefore, because cake permeability is much smaller than the membrane permeability, effective permeability reduction is dominated by cake filtration in the case presented in Figure 8. In this scenario, contrary to the proposed model, the Santos et al. model, 2008; significantly deviates from the experimental data for T=1 (see Figure 8).

Figure 8 - Influence of residual flow and cake filtration on the filtrate volume.

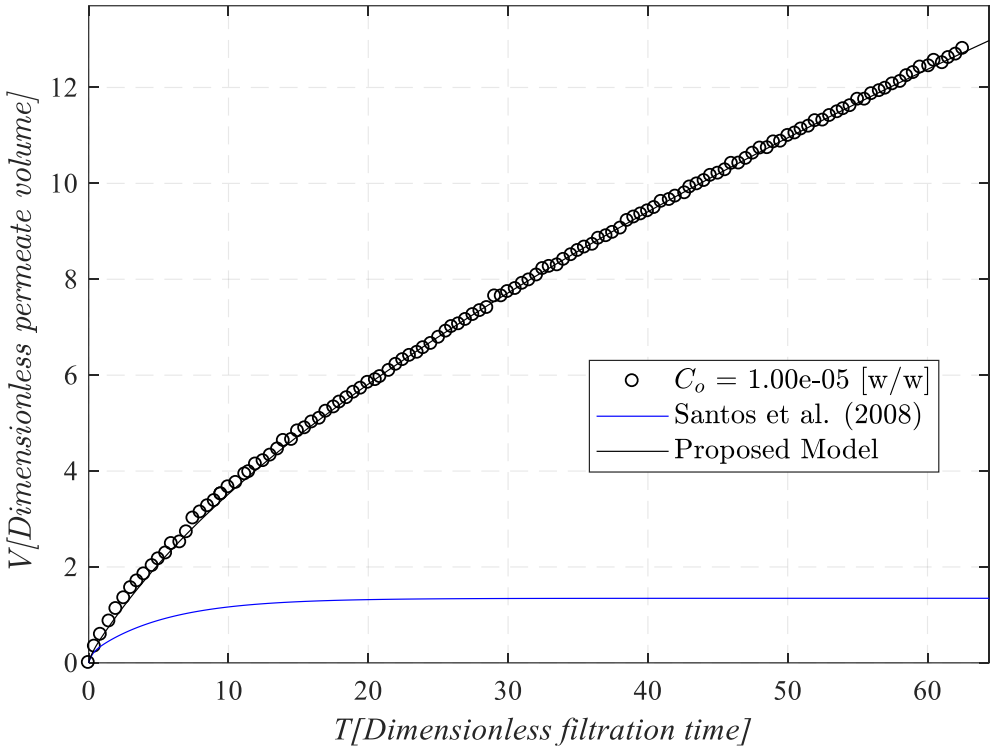

Source: Authors.

Figure 8 presents experimental data fitting for membrane 2 by applying both the proposed and the Santos et al. models, 2008. Contrary to the proposed model, which takes simultaneous pore blocking and cake filtration into account, the Santos et al. model, 2008, incorporates complete pore blocking only, showing that, when all pores are blocked the dimensionless permeate volume tends to be zero.

Figure 9 - Cake build up on membrane 2.

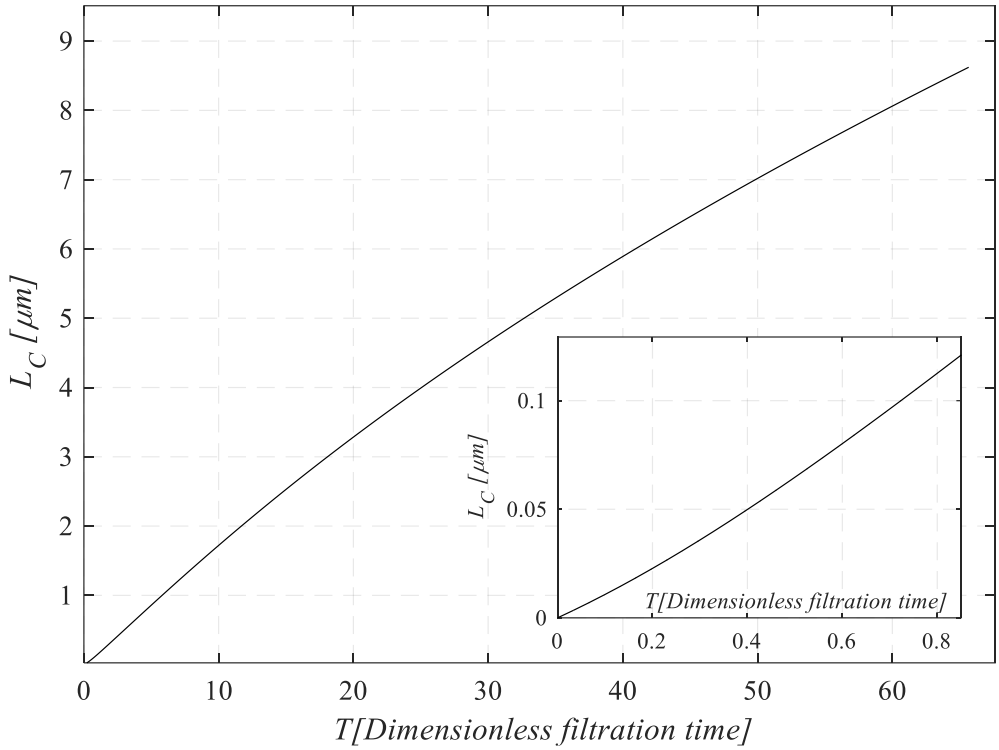

Source: Authors.

Figure 9 shows the cake build up on membrane 2, it can be observed that at the earlier period of injection the cake thickness increases rapidly, as it represents more than 90% of the pores being blocked, after this "transition time", the cake effect on the effective permeability becomes predominant, presenting a stable cake build up tendency.

4. Conclusion

In this article, a model for simultaneous pore blocking and cake filtration (*an integro-differential equation that includes both pore and particle size distributions*) was proposed. The model, which takes pore and particle size distributions into account, was applied for fitting experimental data for filtration on commercial track etched membranes. Although the proposed model considers both filtrations mechanism simultaneously, it was observed that at the beginning of the filtration the straining process is the dominant mechanism, however, through the filtration process this dependence decreases as the open pores are blocked, allowing the cake filtration take control of filtration process. The model thus provides a smooth transition from the pore blockage to the cake filtration behavior during the filtration, avoiding separating mathematical descriptions for different mechanism, unlike most prior pore blockage models. The model showed very good agreement with the studied experimental data, suggesting that the proposed solutions are predictive; i.e, they allow optimizing and designing membrane filtration processes where straining and cake build-up take place simultaneously.

It is recommended to apply the proposed model considering different variables, such as a constant flux and also evaluate it when applied to several industry scenarios, within medical purposes as to oil and gas, only to mention some options.

Acknowledgments

The authors are grateful for the financial support provided by PETROBRAS (grant no. 2017/00249-0). This study was financed in part by the Coordenação de Aperfeiçoamento de Pessoal de Nível Superior – Brasil (CAPES) – Finance Code 001.

Nomenclature

μ	fluid viscosity, $ML^{-1}\ T^{-1}$;
ΔP	pressure drop across the membrane;
L_m	membrane thickness, L;
H	open-pore size distributions, no. L^{-4};
C	suspended-particle size distributions, no. L^{-4};
r_p	pore radius, L;
r_s	particle radius, L;
Q	flow rate per unit of membrane area, $L^3\ T^{-1}$;
Q_{OP}	flow through open pores, $L^3.T^{-1}$;
Q_{BP}	flow through blocked pores, $L^3.T^{-1}$;
A	Membrane area, L^2;
V	filtrate volume, L^3;
h_i	open-pore concentration with radius $r_{p,i}$ per unit of membrane area, no. L^{-3};
c_i	particle concentration with radius $r_{s,i}$ per unit of fluid volume, no. L^{-3};
$r_{s,n}$	radius of the largest particle in suspension;
$r_{p,N}$	radius of the largest pore radius;
$f_{s,j}$	particle size frequency;
k_c	cake permeability, L^{-2};
ϕ_c	cake porosity;
L_c	cake thickness. L;
ε	blocked-to-unblocked pore size ratio;
α^*_{BP}	blocked area fraction.

References

Bolton, G., LaCasse, D., & Kuriyel, R. (2006). Combined models of membrane fouling: Development and application to microfiltration and ultrafiltration of biological fluids, *Journal of Membrane Science. 277, 75–84.*

Bowen W. R., Calvo J. I., & Hernandez A. (1995). Steps of membrane blocking in flux decline during protein microfiltration, *Journal of Membrane Science,* 101, 153.

Filippov A., Starov V. M., Lloyd D. R., Chakravarti S., & Glaser S. (1994). Sieve mechanism of microfiltration, *Journal of Membrane Science.* 89, 199–213.

Gonsalves V. E. (1950). A critical investigation on the viscose filtration. *Rec. Trav. Chim. Des Pays-Bas*, 69, 873.

Goodwin J. W., Hearn J., Ho C. C., & Ottewill R. H. (1974). Studies on the preparation and characterisation of monodisperse polystyrene laticee, *Colloid and Polymer Science*, 252: 464–471.

Grace H. P. (1956). Structure and performance of filter media. *AIChE Journal*, 2.

Herzig J. P., Leclerc D. M., & Le Goff P. (1970). Flow of suspensions through porous media application to deep filtration, Ind. *Eng. Chem.* 62:8–35.

Hermans P. H., & Bredée H. L. (1935). Zur Kenntnis der Filtrationsgesetze, *Recl. Trav. Chim. Pays-Bas*, 54:680–700.

Hlavacek M., & Bouchet F. (1993). Constant flowrate blocking laws and an example of their application to dead-end microfiltration of protein solutions, *Journal of Membrane Science*, 82, 285.

Ho C. C., & Zydney A. L. (2000). A Combined Pore Blockage and Cake Filtration Model for Protein Fouling during Microfiltration, *Journal of Colloid and Interface Science*, 232:389–399.

Kosvintsev S., Cumming I., Holdich R., Lloyd D., & Starov V. (2004). Sieve mechanism of microfiltration separation, Colloids and Surfaces A: *Physicochemical and Engineering*, 230:167–182.

Kosvintsev S., Holdich R., Cumming I., Lloyd D., & Starov V. (2002). Modelling of dead-end microfiltration with pore blocking and cake formation, *Journal of Membrane Science*, 208:181–192.

Polyakov Y. S., & Zydney A. L. (2013). Ultrafiltration membrane performance: Effects of pore blockage/constriction. *Journal of Membrane Science*. 434, 106-120.

Ruth B. F., Montillon G. H., & Montonna R. E. (1933). Studies in Filtration-I. Critical Analysis of Filtration Theory, *Industrial and Engineering Chemistry*, 25(1), 76-82.

Ruth B. F. (1935). Studies in Filtration-III. Derivation of General Filtration Equation, *Industrial and Engineering Chemistry*, 27(6), 708-723.

Santos A., & Bedrikovetsky P. (2006). A stochastic model for particulate suspension flow in porous media, *Transport in Porous Media*, 62:23–53.

Santos A., Bedrikovetsky P., & Fontoura S. (2008). Analytical micro model for size exclusion: Pore blocking and permeability reduction, *Journal of Membrane Scienc*e, 308: 115–127.

Santos A., & Bedrikovetsky P. (2004). Size exclusion during particle suspension transport in porous media: stochastic and averaged equations, *Computational and Applied Mathematics*, 23: 259–284.

Shapiro A. A., Bedrikovetsky P. G., Santos A., & Medvedev O. O. (2007). A stochastic model for filtration of particulate suspensions with incomplete pore plugging, *Transport in Porous Media*, 67:135.

Sharma M. M., & Yortsos Y. C. (1987). Transport of particulate suspensions in porous media: model formulation, *AICHE Journal*, 33:1636-1643.

Tracey E. M., & Davis R. H. (1994). Protein fouling of track-etched polycarbonate microfiltration membranes, *Journal of Colloid and Interface Science*, 1676, 104.